

SuprimeCam Observation of Sporadic Meteors during Perseids 2004

Masanori IYE¹⁻³, Mikito TANAKA², Masahisa YANAGISAWA⁴,
Noboru EBIZUKA⁵, Kouji OHNISHI⁶, Chikako HIROSE⁷

Naoko ASAMI², Yutaka KOMIYAMA¹, and Hisanori FURUSAWA⁸

¹*Optical and Infrared Astronomy Division, National Astronomical Observatory, Mitaka, Tokyo, 181-8588 Japan*
iy@optik.mtk.nao.ac.jp

²*Department of Astronomy, School of Science, University of Tokyo, Tokyo, 113-0033 Japan*

³*Department of Astronomy, Graduate University for Advanced Studies, Hayama, Kanagawa 240-0193 Japan*

⁴*The University of Electro-Communications, Chofugaoka, 1-5-1, Chofu, 182-8585 Tokyo Japan*

⁵*RIKEN, Hirosawa 2-1, Wako, 340-0042 Saitama, Japan*

⁶*Nagano National College of Technology, Tokuma 716, Nagano, 381-8550, Japan*

⁷*Consolidated Space Tracking and Data Acquisition Department,*

Japan Aerospace Exploration Agency (JAXA), 2-1-1 Sengen, Tsukuba, Ibaraki, 305-8505, Japan

⁸*Subaru Telescope, National Astronomical Observatory of Japan, 650 North A'Ohoku Place, Hilo, HI 96720 USA*

(Received 2006 December 20; accepted)

Abstract

We report the serendipitous findings of 13 faint meteors and 44 artificial space objects by Subaru SuprimeCam imaging observations during 11–16 August 2004. The meteors, at about 100km altitude, and artificial satellites/debris in orbit, at 500km altitude or higher, were clearly discriminated by their apparent defocused image sizes.

CCD photometry of the 13 meteors, including 1 Perseid, 1 Aquarid, and 11 sporadic meteors, was performed. We defined a peak video-rate magnitude by comparing the integrated photon counts from the brightest portion of the track traversed within 33 milliseconds (ms) to those from a 0-mag star during the same time duration. This definition gives magnitudes in the range $4.0 < V_{vr} < 6.4$ and $4.1 < I_{vr} < 5.9$ for these 13 meteors. The corresponding magnitude for virtual naked-eye observers could be somewhat fainter especially for the V-band observation, in which the [OI] 5577 line lasting about 1 sec as an afterglow could contribute to the integrated flux of the present 5–10 min CCD exposures.

Although the spatial resolution is insufficient to resolve the source size of anything smaller than about 1 m, we developed a new estimate of the collisionally excited column diameter of these meteors. A diameter as small as a few mm was derived from their collisionally excited photon rates, meteor speed, and the volume density of the oxygen atoms at the 100km altitude. The actual column diameter of the radiating zone, however, could be as large as few 100m because the excited atoms travel that distance before they emit forbidden lines in 0.7 sec of its average lifetime.

Among the 44 artificial space objects, we confirmed that 17 were cataloged satellites/space debris. This shows the usefulness of SuprimeCam wide-field imaging programmed to study the faint meteor population and faint space debris.

Key words: meteor — Perseids, photometry

1. Introduction

Scientific observation of meteors is not a simple task because of the difficulty in predicting their appearance in time and position. The brightness of a meteor depends on the size and the velocity of the meteoroid. Typical meteors seen by the naked eye or by video cameras are caused by meteoroids larger than about 0.01mm (Ceplecha et al. 1998). However, the luminosity distribution of meteors at its fainter end is not well-known. Moreover, the scientific definition of the magnitude of meteors is not well established because of the variety of parameters involved in making observations, for example, the speed and distance of the meteor and the spatial and spectral resolution and the spatial and spectral coverage of the instrument used,

which can be the naked-eye, a video camera, an intensified camera, a CCD camera, or another device.

Hawkins and Whipple (1958) and Cook et al. (1962) evaluated the width of meteor trails by comparing the measured trail width on photographs with those of stars and derived a typical value in the order of 1m. Note that this evaluation is from broadband images and the decomposition analysis is a rather delicate process, as indicated by some nominal negative values that were derived in Hawkins and Whipple (1958). Kaiser et al. (2004) made two station, short-baseline (≤ 100 m) high resolution measurements of 34 faint meteoroids to evaluate the trail width using intensified CCD cameras and found that their FWHM were generally less than 1m. Jenniskens et al. (2004) serendipitously obtained an extended spectrum

of a meteor trail with FORS1 on VLT but the apparent extension turned out to be caused by the defocus effect and the meteor was not spatially resolved.

The present paper reports the serendipitous observation of meteors made with the wide-field SuprimeCam of the 8.2m Subaru Telescope during the Perseid meteor shower of 2004.

Perseid meteors are known to be associated with the parent comet 109P/Swift–Tuttle, which was first recorded in BC 68 and returns every 135 years with recent visits in 1862 and 1992. The perihelion of 109P/Swift–Tuttle remained outside the Earth’s orbit for at least for last 2000 years, but the current perihelion is at 0.958 AU. Its orbit is highly eccentric $e = 0.963$ and highly inclined $i = 113^\circ.4$ with the velocity relative to the Earth as large as about 60 km/s (Lyytinen and Van Flandern 2004). When it comes close to the Sun, a new trail is produced; at least five such dust trails are known from passages corresponding to AD 1348, 1479, 1610, 1737, and 1862. Taking the perturbation of Jupiter, Saturn and other planets into account, Lyytinen and van Flandern (2004) calculated that the one-revolution dust trail from the 1862 encounter passed within 0.0013 AU from the Earth’s orbit at about 21 UT on 11 August 2004.

2. Observations and Data Reduction

The data used were obtained serendipitously during observations on other projects. Broadband imaging observations of M31 and narrowbands imaging observations of the Subaru Deep Field were made with the SuprimeCam (Miyazaki et al. 2002) attached at the prime focus of the Subaru Telescope (Iye et al. 2004) during four nights, 12–15 August 2004, Hawaiian Standard Time (HST=UT-10), shortly after the expected epoch of Perseid meteor events.

During the course of these observations, we serendipitously noticed several tracks recorded on the CCD images. Although no elaborate statistical assessment of the mean rate of meteor/artificial satellite tracks recorded on SuprimeCam was available at that time and although we didn’t know how to securely discriminate meteors and artificial satellites without having double-station observations, we suspected that the event rate observed during this period could be significantly larger than the average. Although we recognized that some of these recorded tracks must have been artificial satellites, we took a closer look. We asked SuprimeCam observers on the preceding four nights, 8–11 August, including the Perseid peak epoch, to check their images as well; one of these observers, I. Iwata, reported finding nine tracks in his images. Two other observers who conducted SuprimeCam imaging did not find such tracks during this period.

Table 1 summarizes the observational parameters of all of the detected tracks recorded during eight nights of SuprimeCam observation, 8–16 August 2004, HST. Tracks #1–#9 were reported by I.Iwata. Tracks #10–#43 were noticed by one of our authors, M.T., while taking a quick look at the observed images onsite. Tracks #44–#56 also were later noted by M.T. while reducing the imaged data.

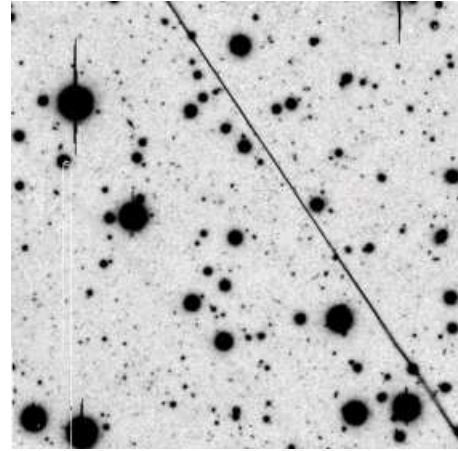


Fig. 1. Track #11_812_39_8

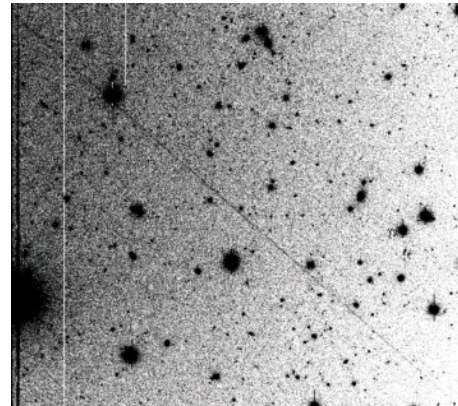


Fig. 2. Track #50_813_56_5

Track #57 was found by M.I. while reducing the meteor images for this paper. Eventually, this eight-night series of SuprimeCam observations yielded 57 tracks.

A short explanation of each column follows:

- Column (1): Sequential number #
- Column (2): Start time of exposure in HST
- Column (3): Frame number of the night
- Column (4): CCD file number SUPA00nnnnnn (10 files starting from this number constitute the entire SuprimeCam field of view (FOV) covered with 10 CCDs)
- Column (5): Right ascension in degrees
- Column (6): Declination in degrees
- Column (7): Azimuth angle in degrees
- Column (8): Elevation angle in degrees
- Column (9): Filter band
- Column (10): Exposure time in seconds
- Column (11): Total track length l in pixels over several CCDs
- Column (12): Position angle θ of the track
- Column (13): Full width half maximum (FWHM) w in arcsec
- Column (14): Average peak count per pixel in ADU.
- Column (15): Nominal integrated magnitude for the

(1)	(2)	(3)	(4)	(5)	(6)	(7)	(8)	(9)	(10)	(11)	(12)	(13)	(14)	(15)
#	ExpStart HST h m s	Fr No.	CCDFr SUPA00-	RA deg	Dec deg	Az deg	El deg	Fil	Exp sec	l pix	θ deg	w "	I_p ADU	m_{nom}
1	08/11 04 03 58	-	-	14.0	12.5	-	-	V	600	2873	11.8	-	-	
2	08/11 04 14 58	-	-	14.0	12.5	-	80.0	V	600	4235	-16.4	-	-	
3	08/12 01 53 08	-	-	14.0	12.5	-	-	V	600	2683	48.0	-	-	
4	08/12 02 04 08	-	-	14.0	12.5	-	-	V	600	2004	77.8	-	-	
5	08/12 02 26 10	-	-	14.0	12.5	-	-	V	600	1993	71.6	-	-	
6	08/12 03 10 13	-	-	14.0	12.6	-	-	V	600	2186	-65.7	-	-	
7	08/12 03 32 14	-	-	14.0	12.6	-	-	V	600	3994	-0.7	-	-	
8	08/12 03 32 14	-	-	14.0	12.6	-	81.0	V	600	4082	-12.8	-	-	
9	08/12 03 32 14	-	-	14.0	12.6	-	81.0	V	600	2353	-56.6	-	-	
10	08/13 00 23 14	38	337990	15.0	38.9	55.1	41.2	V	600	2801	-13.8	1.0	120	19.6
11	08/13 00 34 14	39	338000	15.0	38.9	54.7	43.3	V	600	7430	33.3	2.6	380	17.4
12	08/13 01 08 12	42	338030	19.3	38.7	53.0	49.5	V	600	6462	12.1	1.4	500	17.6
13	08/13 03 42 05	64	338250	15.0	38.9	6.5	70.8	Ic	300	2178	23.6	1.0	120	18.4
14	08/13 03 48 27	65	338260	14.0	39.2	0.3	70.6	Ic	300	2773	-39.5	1.2	60	19.1
15	08/13 03 54 27	66	338270	14.0	39.2	356.8	70.5	Ic	300	3363	23.5	1.2	3200	14.7
16	08/13 04 06 29	68	338290	14.0	39.2	349.9	70.2	Ic	300	5218	-31.9	1.6	1800	15.1
17	08/13 04 12 30	69	338300	14.3	39.2	346.6	69.9	Ic	300	2793	34.8	13.6	38	16.9
18	08/13 04 54 40	76	338370	7.6	38.1	318.2	63.4	Ic	300	6368	-33.3	2.6	1250	15.0
19	08/14 00 42 21	37	338900	13.6	39.5	53.0	46.5	V	600	6609	22.9	12.2	195	16.4
20	08/14 00 53 22	38	338910	13.6	39.5	52.0	48.6	V	600	6386	45.8	1.4	420	17.9
21	08/14 01 37 29	42	338950	12.9	39.9	2.0	56.8	V	600	4057	-61.3	1.4	2000	16.2
22	08/14 01 37 29	42	338950	12.9	39.9	46.0	56.8	V	600	7191	29.0	1.4	480	17.7
23	08/14 03 26 47	59	339120	11.9	39.1	5.7	70.6	Ic	300	4189	47.9	13.4	55	16.5
24	08/14 03 44 55	62	339150	7.3	37.8	343.6	71.1	Ic	300	5060	-72.6	1.6	800	15.9
25	08/14 04 33 24	70	339230	17.3	37.6	338.4	70.6	Ic	300	7533	-65.5	13.4	120	15.7
26	08/14 20 18 11	4	339460	197.3	27.5	290.5	33.3	N	900	4795	-59.2	6.0	95	19.3
27	08/14 21 08 13	9	334520	315.1	6.3	104.9	50.6	Ic	300	3680	80.6	13.8	70	16.3
28	08/14 21 26 22	12	339540	315.1	6.3	106.9	53.4	Ic	300	8489	-24.4	1.0	500	17.1
29	08/14 21 38 23	14	339560	315.1	6.3	109.2	56.1	Ic	300	4534	-20.2	1.0	180	18.1
30	08/15 02 33 54	46	339880	14.0	39.2	33.1	65.8	V	600	4081	-49.9	12.6	125	15.7
31	08/15 03 12 11	50	339920	12.2	40.4	11.5	68.9	Ic	300	9881	-80.8	2.2	1400	15.0
32	08/15 20 17 21	5	340220	197.3	27.5	290.6	32.7	N	900	4894	61.8	1.2	420	17.0
33	08/15 22 39 15	23	340400	253.0	34.9	300.3	46.6	V	600	5375	-13.0	6.0	350	18.5
34	08/16 00 23 14	32	340490	13.3	39.7	233	45.0	V	600	3441	52.1	14.8	22	18.5
35	08/16 01 29 19	38	340550	17.6	37.4	232	55.0	V	600	7796	-26.5	1.4	1300	16.6
36	08/16 02 59 42	45	340620	17.6	37.4	207	70.0	Ic	300	7538	-19.5	1.4	200	17.7
37	08/16 03 17 49	48	340650	15.0	40.4	184	70.0	Ic	300	7990	5.9	1.2	230	17.6
38	08/16 03 41 51	52	340690	15.0	40.4	184	70.0	Ic	300	7792	3.8	1.4	1900	15.2
39	08/16 03 59 52	55	340720	13.3	39.7	166	69.0	Ic	300	3597	24.2	2.6	30000	11.5
40	08/16 04 05 53	56	340730	13.3	39.7	166	69.0	Ic	300	5679	-32.3	13.0	70	16.3
41	08/16 04 23 56	59	340760	13.3	39.7	166	69.0	Ic	300	7718	-7.5	2.4	240	16.8
42	08/16 04 29 57	60	340770	12.1	38.8	149	67.0	Ic	300	5332	-8.6	2.0	1400	15.1
43	08/16 04 47 56	63	340800	12.1	38.8	149	67.0	Ic	300	4300	40.8	14.4	35	17.0
44	08/15 03 24 13	52	339940	12.2	40.4	5.1	69.3	Ic	300	2371	-55.3	12.0	38	17.1
45	08/13 03 48 27	65	338260	14.0	39.2	0.3	70.5	Ic	300	1820	-39.6	1.4	80	18.6
46	08/13 04 06 29	68	338290	14.0	39.2	349.8	70.2	Ic	300	3274	-16.6	2.0	1080	18.0
47	08/14 01 15 23	40	338930	12.9	39.9	49.0	52.9	V	600	1195	54.1	0.8	20	21.8
48	08/14 03 20 44	58	339110	11.9	39.1	9.1	70.4	Ic	300	2315	-23.0	1.4	170	17.7
49	08/14 04 03 05	65	339180	7.3	37.8	333.8	69.5	Ic	300	3748	13.5	1.0	30	20.1
50	08/14 04 15 07	56	339200	7.3	37.8	328.5	68.1	Ic	300	2539	-48.9	1.4	170	17.8
51	08/15 01 05 45	38	339800	17.3	37.6	54.7	49.4	V	600	3894	-10.9	0.8	70	20.5
52	08/16 04 23 56	59	340760	13.3	39.9	334.4	67.4	Ic	300	2661	44.9	13.0	16	17.9
53	08/16 04 23 56	59	340760	13.3	39.9	334.4	67.4	Ic	300	1399	-29.2	1.0	40	18.9
54	08/13 20 42 50	11	338640	313	6.0	101.8	45.0	Ic	300	2212	60.8	14.6	48	16.6
55	08/13 20 48 51	12	338650	313	6.0	102.6	47.0	Ic	300	2496	37.0	1.6	700	16.1
56	08/15 03 36 15	54	339960	13.3	39.9	6.2	71.0	Ic	300	1420	18.1	2.0	100	18.0
57	08/15 02 33 54	46	339880	14.0	39.2	33.1	65.7	V	600	2983	44.0	13.2	16	19.0

Table 1. Faint tracks recorded during 10-16 August, HST

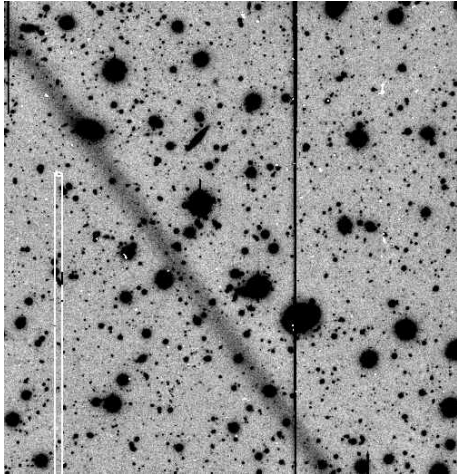


Fig. 3. Track #17_812_69_8

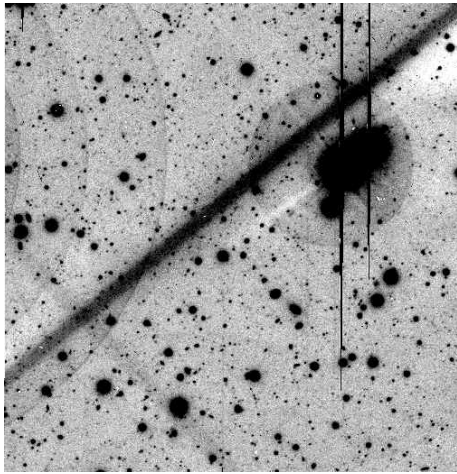


Fig. 4. Track #30_814_46_9 (brighter one) and #57_814_46_9 (fainter one)

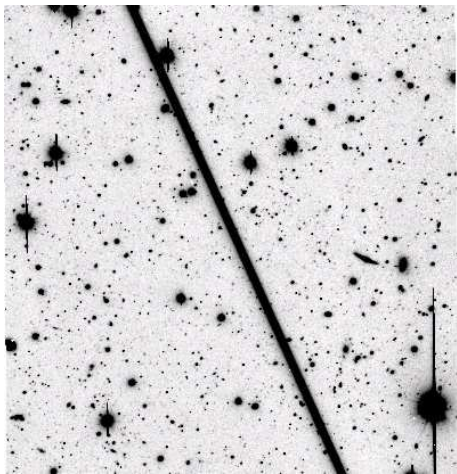


Fig. 5. Track #39_815_55_5

brightest 5 arcmin portion. See section 4 for further details.

Figures 1 to 5 show typical images among the recorded 57 tracks. The figure 1 labeled #11_812_39_8, for example, shows about 1800×1800 pixel portion of the image of track #11 recorded on the 8th CCD of the 39th exposure frame taken on 12 August, HST. To elucidate the tracks, the surface brightness ranges of these images were adjusted individually to give high contrast.

As will be explained later, Figure 1 was identified as satellite COSMOS 2363 = ID98077B = NORAD#25594, flying at a high orbit with a slant range 20,000 km and an orbiting period of 675.73 min. The brightness variation in this frame is visible because of the rotation of the satellite. Similar light modulation along the track was noticed also for #5, #36, and #45.

Figure 2 is another satellite DIAMANT_B-P4 = ID75010A = NORAD#07654, flying at a low orbit, below 1500 km, with an orbital period 107.69 min.

Figure 3 is a Perseid meteor at a distance of about 106 km. The track is blurred because of the significant defocus effect that occurs when the SuprimeCam is focused to infinity.

Track #30 in Figure 4 is a sporadic meteor. This meteor exhibited an outburst in which its luminosity increased by a factor of seven during its passage through the SuprimeCam FOV. Another even fainter track of #57 crossing almost orthogonally to #30 is seen in the lower left corner of this image.

Figure 5 is the brightest saturated satellite image among the sample.

The usual procedures were taken to subtract bias, and flat-fielding the raw frames was performed using the SuprimeCam Data Reduction package SDFRED (Yagi et al. 2002; Ouchi et al. 2004).

3. Meteor Identification

3.1. Image Width

An object with a diameter D at a distance d from the telescope, imaged by the SuprimeCam with focal length f focused to the infinity under a typical seeing of s in radian, will have an image size w , as given by

$$w = \sqrt{f^2 D^2 d^{-2} + \delta^2 F^{-2} + f^2 s^2}, \quad (1)$$

where the second term denotes the blurred image size due to the defocus δ of a beam with focal ratio $F = 2$ given by

$$\delta = f^2 / (d - f). \quad (2)$$

Note that the pixel scale of SuprimeCam is 0.20 arcsec/pixel with $15\mu\text{m}$ pixel.

Figure 6 shows the calculated FWHM image width (in arcsec) as a function of distance d under typical seeing size of 0.8 arcsec ($s = 4 \times 10^{-6}$ radian) for objects with size $D=1\text{m}$, 3m, and 10m. At the distance of meteors, 100 km $< d < 200$ km, the second term of the defocus effect is the leading term; the defocused images of meteors should have an image size larger than 8 arcsec at a distance of

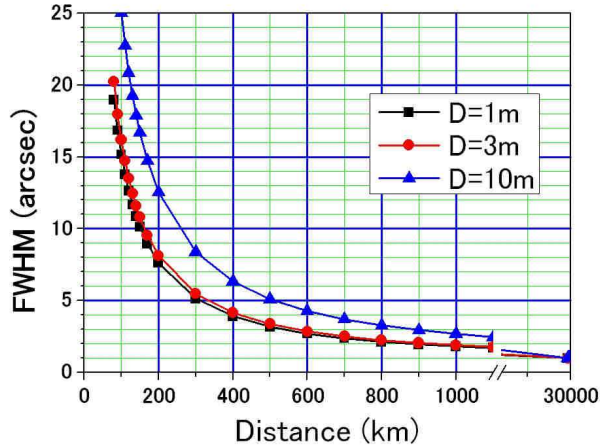


Fig. 6. FWHM size of the defocused object of diameter D at a distance d from the telescope under a typical seeing size of 0.8 arcsec. Objects smaller than 1m in size are not resolved at 100km distance.

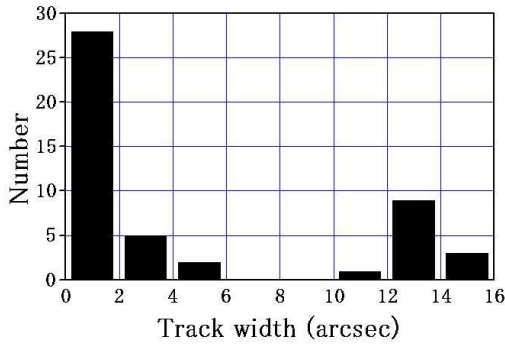


Fig. 7. Bimodal FWHM size distribution of the detected tracks.

less than 200 km. Note that size information of an object smaller than 1 m cannot be retrieved from its defocused image width.

Figure 7 shows the actual FWHM track width distribution of the 48 measured tracks. The distribution shows a clear separation of the two populations. Thirteen tracks are wider than 10 arcsec and correspond to meteors and the remaining 35 tracks are narrower than 6 arcsec and correspond to satellites and space debris.

3.2. Position Angle

Several meteor groups are known to appear during the time period of the observations as shown in Table 2. Cassiopeids are considered to be a parted family of Perseids.

We performed a cross-check to determine if the position angles of the observed tracks point to any of the radiant points of these meteor groups. Table 3 summarizes the results of the meteor identification and lists some of the physical parameters that were measured for these 13 meteor tracks. An explanation of the procedures adopted to derive the physical parameters is given after the short description of each column:

- Column (1): Sequential ID number
- Column (2): Exposure start time in UT(=HST+10h)

(1)	(2)	(3)	(4)	(5)
Group	Period	Max	RA	Dec
γ Per	23 Jul.-23 Aug.	12 Aug.	47°	58°
(N) δ Aqr	7 Jul.-25 Aug.	12 Aug.	340°	-5°
(S) δ Aqr	21 Jul.-29 Aug.	29 Jul.	334°	-16°
(N) ι Aqr	15 Jul.-20 Sep.	20 Aug.	328°	-6°
(S) ι Aqr	15 Jul.-25 Aug.	4 Aug.	334°	-15°
α Cap	15 Jul.-10 Aug.	31 Jul.	308°	-10°
Cas	17 Jul.-15 Aug.	28 Jul.	15°	63°
κ Cyg	19 Aug.-25 Aug.	-	289°	55°

Table 2. Meteor groups active during 10-16 August.

Column (3): Elevation angle

Column (4): Distance to the meteor assuming an altitude of 100 km from the ground

Column (5): Filter band used for imaging

Column (6): FWHM w of the track in pixels

Column (7): Average peak count I_p per pixel in ADU

Column (8): Observed position angle θ of the meteor track

Column (9): Angle deviation $\delta\theta_{Per}$ from γ Per radiant point

Column (10): Angle deviation $\delta\theta_{Aqr}$ from (N) δ Aqr radiant point

Column (11): Meteor group identification. Per; Perseids, δ Aqr; δ Aqr(N), Spo; sporadic. Although possible associations to Perseids and Aquarids are not completely denied, we consider the nine meteors with "Spo/P?", and "Spo/A?" denotation to be sporadic meteors, based on the sporadic meteor event rate as described in the discussion.

Column (12): Angle distance Ψ of the telescope pointing from the radiant point.

Column (13): Meteor angular speed Ω . Except for Perseid #17 and Aquarid #25, we adopted a canonical angular speed of 10°/s for sporadic meteors to simplify matters.

Column (9) of Table 3 shows the deviation of the position angle $\delta\theta_{Per}$ of the track from the nominal Perseid radiation point. For the daily radiant ephemeris for the Perseid meteor showers, we refer to Arlt (2003) and Lyytinen and van Flandern (2004).

The spread in Perseid radiants was estimated to be about 2-3 degrees wide (cf. Jones and Sarma 1979; Lindblad and Porubcan 1995; Molau and Arlt 1997). The analysis of Perseid meteors observed in 1997 (Shigeno et al.; <http://www004.upp-so-net.ne.jp/msswg/Ob970812.txt>), showed that the actual distribution of the radiant points of 23 bright meteors, with magnitudes ranging from 0.5 – 8.5 mag and mean magnitude 4.76, spread about 3°, while a fainter group of 14 meteors in the range 6 – 8.5 mag, with mean magnitude 7.00, spread in a much wider region, 60° in right ascension and 20° in declination. This suggests that the radiant points of fainter meteors may spread much wider in space.

Track #17 is aligned to the position angle of the Perseid radiant point within 1°, and we associate this meteor with the Perseids. Tracks #43, 52, 57, 19, 23, and 34 are within 15° from the direction of the Perseid radiant point and although some may be Perseids, considering the finding of Shigeno et al.(1997), we prefer to consider them sporadic meteors based on the mean event rates independently evaluated in other fields.

Column (10) shows the angle deviation $\delta\theta_{Aqr}$ to (N) δ Aqr meteor radiation point. Here, we identify track #25, whose track position angle is pointing within 3° from the Aquarid

(1)	(2)	(3)	(4)	(5)	(6)	(7)	(8)	(9)	(10)	(11)	(12)	(13)
ID	ExpStart	EL	d	B	w	I_p	θ	$\delta\theta_{Per}$	$\delta\theta_{Aqr}$	group	Ψ	Ω
#	UT h m s	deg	km		pix	ADU	deg	deg	deg		deg	$^{\circ}/s$
17	8/13 14 12 30	69.9	106	Ic	68	38	35.5	-0.4	-81.6	Per	29	15.5
54	8/14 06 42 50	45.0	141	Ic	73	48	-60.8	-81.1	29.7	Spo	-	10:
19	8/14 10 42 21	46.5	138	V	61	195	23.5	-13.0	85.2	Spo/P?	-	10:
23	8/14 13 26 47	70.6	106	Ic	67	55	48.0	11.3	-72.4	Spo/P?	-	10:
25	8/14 14 33 24	70.6	106	Ic	67	120	-66.0	81.2	2.3	δAqr	62	10.2
27	8/15 05 08 13	50.6	129	Ic	69	70	80.6	60.0	-6.0	Spo/A?	-	10:
30	8/15 12 33 54	65.8	110	V	63	125	-51.0	-87.0	11.5	Spo/A?	-	10:
57	8/15 12 33 54	65.8	110	V	66	16	44.0	8.0	-73.5	Spo/P?	-	10:
44	8/15 13 24 13	69.3	107	Ic	60	38	-55.0	86.9	4.0	Spo/A?	-	10:
34	8/16 10 23 14	45.0	141	V	74	22	52.1	15.2	-66.8	Spo/P?	-	10:
40	8/16 14 05 53	69.0	107	Ic	65	70	-32.3	-69.2	28.8	Spo	-:	10:
52	8/16 14 23 56	67.0	108	Ic	65	16	45.0	7.9	-74.1	Spo/P?	-	10:
43	8/16 14 47 56	67.0	109	Ic	72	35	41.3	5.0	-78.5	Spo/P?	-	10:

Table 3. Meteors recorded during 10–16 August in their order of appearance.

radiant point, with this group of meteoroids. Again, some of the tracks #27, 44, and 30, with angle deviation less than 12° , might also be members of this group, or other nearby Aquarid groups, (S) δAqr , (N) ιAqr , or (S) ιAqr , as shown in Table 2. Note that the position angle matched best to (N) δAqr for all four tracks. We interpret that all of the meteors except track #25 are largely sporadic, according to the same reasoning.

The remaining two, #40 and 54, did not match the radiant points of the groups listed in Table 2 and are considered here to be secure sporadic meteors. The number of sporadic meteors in our sample is therefore at most 11.

Figures 8 and 9 show the identified meteor tracks recorded in several contiguous CCDs. Contrast levels were adjusted individually to make the tracks visible. Some of the meteors showed significant changes in their luminosity during their passage of the SuprimeCam FOV. The luminosity profile of these images is discussed in section 4.2. Note that doubly split images of meteors #27 and #43 are due to the defocused central obscuration of the telescope.

The distance d to the meteor is given in column (4) of Table 3 using the relation $d = H/\sin(\text{El})$, where the luminous altitude $H=100$ km was assumed. The angular speed, Ω , of the meteor entering the luminous height at a velocity v with an angular separation Ψ , from the radiant point is given in column (13) by

$$\Omega = v \sin(\Psi)/d, \quad (3)$$

for a Perseid and an Aquarid meteor, respectively. For other sporadic meteors, we adopted a common canonical value of 10 degrees/sec, for simplicity.

4. Photometry

4.1. Absolute photometry and nominal CCD magnitude

We performed absolute photometry of the CCD frames by imaging twice in each night two of the following four photometric standard star fields, SA110, SA92, PG2332+055, and MARK(Landolt 1999). The photometric zero points of V-band and Ic-band were established by 14 to 24 standard stars in the magnitude range $11.8 \leq V \leq 16.3$ and $10.7 \leq Ic \leq 15.3$ available in each shot.

For example, the Ic-band zero point of the CCD frame SUPA00338307 for #17 and SUPA00339230 for #25 were 33.39 and 33.39 mag, respectively. The V-band zero point

of SUPA00339888 for #30 and SUPA00338900 for #19 were 34.47 and 34.48 mag respectively. The deviation of these zero points was well less than 0.1 mag.

Table 4 summarizes the photometric properties of the 13 meteoroids. Definition of columns (1) to (5) are common to those in Table 3. Column (6) denotes the nominal integrated magnitude, $m_{5'}^{nom}$, of the brightest 5 arcmin portion of the track, as derived by comparing the integrated ADU counts,

$$F_{5'}^{nom} = wI_p \times 1500, \quad (4)$$

where the factor 1,500 is the number of pixels along the 5 arcmin portion of the track with those of standard stars for longer integration time. For example, the Perseid meteor #17 has $wI_p = 2584 \text{ADU/pixel}$, and the total ADC $F_{5'}$ within the brightest 5 arcmin track length is 3.9×10^6 .

The nominal magnitudes are given by

$$V_{5'}^{nom} = -2.5 \log(F_{5'}^{nom}) + 34.47, \quad (5)$$

and

$$I_{5'}^{nom} = -2.5 \log(F_{5'}^{nom}) + 33.39. \quad (6)$$

Note that this is a *nominal* magnitude because CCD photometry for temporary luminous objects like meteors gives apparently fainter nominal magnitudes for CCD images with longer exposure times.

To characterize the meteor magnitude more quantitatively, taking into account its luminous time, we introduce a possible definition of meteor magnitudes in column (8) by calculating/assuming the meteor angular velocity. This is discussed in sections 4.2 and 4.3. The physical meaning of column (9) is discussed in section 5.1.

Column (1): Sequential ID number

Column (2): Exposure start time in UT(=HST+10h)

Column (3): Filter band used for imaging

Column (4): wI_p in ADU per unit pixel along the track

Column (5): Meteor group identification

Column (6): Nominal magnitude, see text above

Column (7): Meteor angular speed Ω . For sporadic meteors, we assumed a canonical angular speed of $10^{\circ}/s$ to give the estimated values for columns (8) and (9).

Column (8): Video-rate magnitude m_{vr} defined as V_{vr} or I_{vr} . This magnitude corresponds to the spatial integration of all of the photons from the portion of the track length traversed within 0.033 sec. See section 4.2. Note that this includes, for



Fig. 8. Meteor tracks

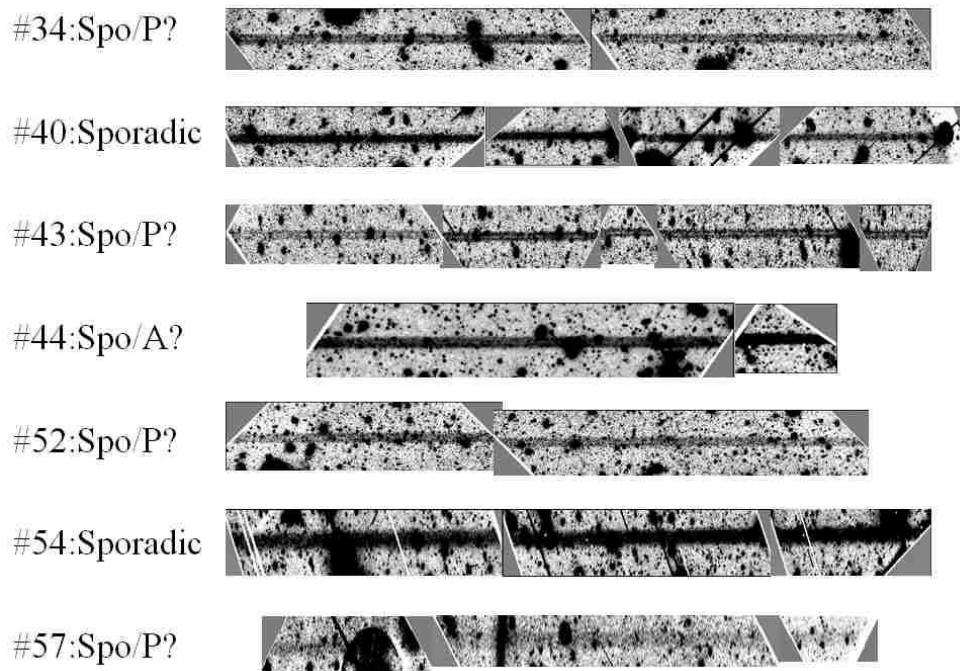


Fig. 9. Meteor tracks

(1)	(2)	(3)	(4)	(5)	(6)	(7)	(8)	(9)
ID	ExpStart	B	wI_p	group	$m_{5'}^{nom}$	Ω	m_{vr}	D_{col}
#	UT h m s		ADU		mag	$^{\circ}/s$	mag	mm
17	8/13 14 12 30	Ic	2584	Per	16.9	15.5	4.9	-
54	8/14 06 42 50	Ic	3504	Spo	16.6	10:	5.0:	-
19	8/14 10 42 21	V	11895	Spo/P?	16.4	10:	4.2	10.3
23	8/14 13 26 47	Ic	3685	Spo/P?	16.5	10:	5.0	-
25	8/14 14 33 24	Ic	8040	δ Aqr	15.7	10.2	4.1	-
27	8/15 05 08 13	Ic	4830	Spo/A?	16.3	10:	4.7	-
30	8/15 12 33 54	V	7875	Spo/A?	15.7	10:	4.6	6.7
57	8/15 12 33 54	V	1056	Spo/P?	19.0	10:	6.8	2.4
44	8/15 13 24 13	Ic	2280	Spo/A?	17.1	10:	5.5	-
34	8/16 10 23 14	V	1628	Spo/P?	18.5	10:	6.4	3.9
40	8/16 14 05 53	Ic	4550	Spo	16.3	10:	4.8:	-
52	8/16 14 23 56	Ic	1040	Spo/P?	17.9	10:	6.4	-
43	8/16 14 47 56	Ic	2520	Spo/P?	17.0	10:	5.4	-

Table 4. Physical characteristics of meteors recorded.

the V-band, the afterglow contribution from [OI]5577 lasting about 1 sec.

Column(9): Calculated maximum diameter of collisionally excited meteors column D_{col} . See section 5.1 for further details.

4.2. Video-rate magnitude

The number of 0.2 arcsec pixels that span a video frame of 0.033 sec, for a meteor with angular speed Ω deg/s is $3600 \times 0.033\Omega/0.2 = 590\Omega$ pixels. The total ADC for the brightest observed part of the track F_{vr} in 33 msec is then

$$\begin{aligned} F_{vr} &= wI_p \times 590 \times \Omega \\ &= F_{5'}^{nom} \times \Omega \times 590/1,500, \end{aligned} \quad (7)$$

where wI_p is the average ADU count integrated perpendicularly across the track over the blurred image of the meteor given in column (4) of Table 4. For example, the Perseid meteor #17 has $wI_p = 2584$ ADU/pixel and an angular speed of $\Omega = 15.5^{\circ}/\text{sec}$ at an elevation angle $EL = 70^{\circ}$. The total ADC F_{33} within a video-rate frame, corresponding to a track length of 0.52° , or 9,200 pixels, would then be about 2.4×10^7 .

We define the video-rate magnitudes V_{vr} and I_{vr} by

$$V_{vr} = V_{5'} - 2.5\log(\Omega) - 9.64, \quad (8)$$

and

$$I_{vr} = I_{5'} - 2.5\log(\Omega) - 8.88, \quad (9)$$

where the offsets of 9.64 and 8.88 correspond to the magnitude differences $2.5 \log(600/0.033 \times 590/1500)$ and $2.5 \log(300/0.033 \times 590/1500)$, respectively.

These values are shown in column (8) of Table 4. Note that the actual video-rate magnitude could be somewhat fainter than the values given in column (8) as this magnitude is calculated assuming that the brightness remains at a constant maximum value throughout the 0.033sec.

4.3. Magnitude Linking to Visual Estimation

Note, however, that the magnitude m_{vr} given here cannot be linked well to the magnitudes reported by most of eye-witness observers. Quantitative comparison between the "integrated" meteor brightness and background stars is not straightforward because the effective length of integration time corresponding to the eye response time and the residual memory time has not been well calibrated. The eye-witness magnitude may give a

much fainter value than the currently introduced photometric definitions of meteor magnitude, m_{vr} . Another physical factor to be considered in calibrating magnitudes is the time profile of meteor radiation. Because a small, but significant, fraction of the photons in the V-band is emitted at the [OI] 5577A forbidden line that lasts 1–3 sec, the actual duration of emission recorded in the present observation would be longer than the adopted video-rate and hence the actual magnitude corrected for this afterglow duration time, m_{cor} , could be at most 2–3 mag fainter than V_{vr} . In the I_c band, where the OI 7774A and N_2 bands are dominant and no significant forbidden line contributes, such an afterglow effect would be negligible.

Therefore, most of the currently observed meteors could possibly be as faint as 7–8 mag to visual observers. However, we will not pursue a rigorous quantitative calibration between eye estimate magnitudes and the photon counting magnitude in this paper.

4.4. Luminosity Profiles

Figures 10 and 11 present a luminosity profile scanned along the track of all of the recorded meteors. The ADU count averaged over the FWHM is shown in these plots. Bright spikes in the profile are due to stars and/or hot pixels and the lower envelope of the profile indicates the meteor luminosity. Some of the meteors, for example, #19 and #23, show fairly constant brightness. However, the meteor #30 flared up by a factor of 7 in brightness and meteor #27 showed a gradual change in luminosity by a factor of 3 within the recorded frame. The FWHM track length for the flare-up of meteor #30 is about 500 arcsec (= 2500 pixels), corresponding to an elapsed time of 14 msec. This event could be employed to constrain the ablation process through the use of an appropriate model.

5. Discussion

5.1. Rate of Sporadic Meteors

To evaluate the rate of sporadic meteors, we examined 209 SuprimeCam frames (2090 CCD images) obtained for the Subaru Deep Field (SDF) during 2001–2004, which are publicly available in the Subaru data archive. 173 frames are in the I' band with an exposure time of 210 to 300 sec, and 46 frames are in the V band with an exposure time 720 to 900 sec. Most of the exposures were taken in March, April, and May. The total exposure time of these frames amounted to

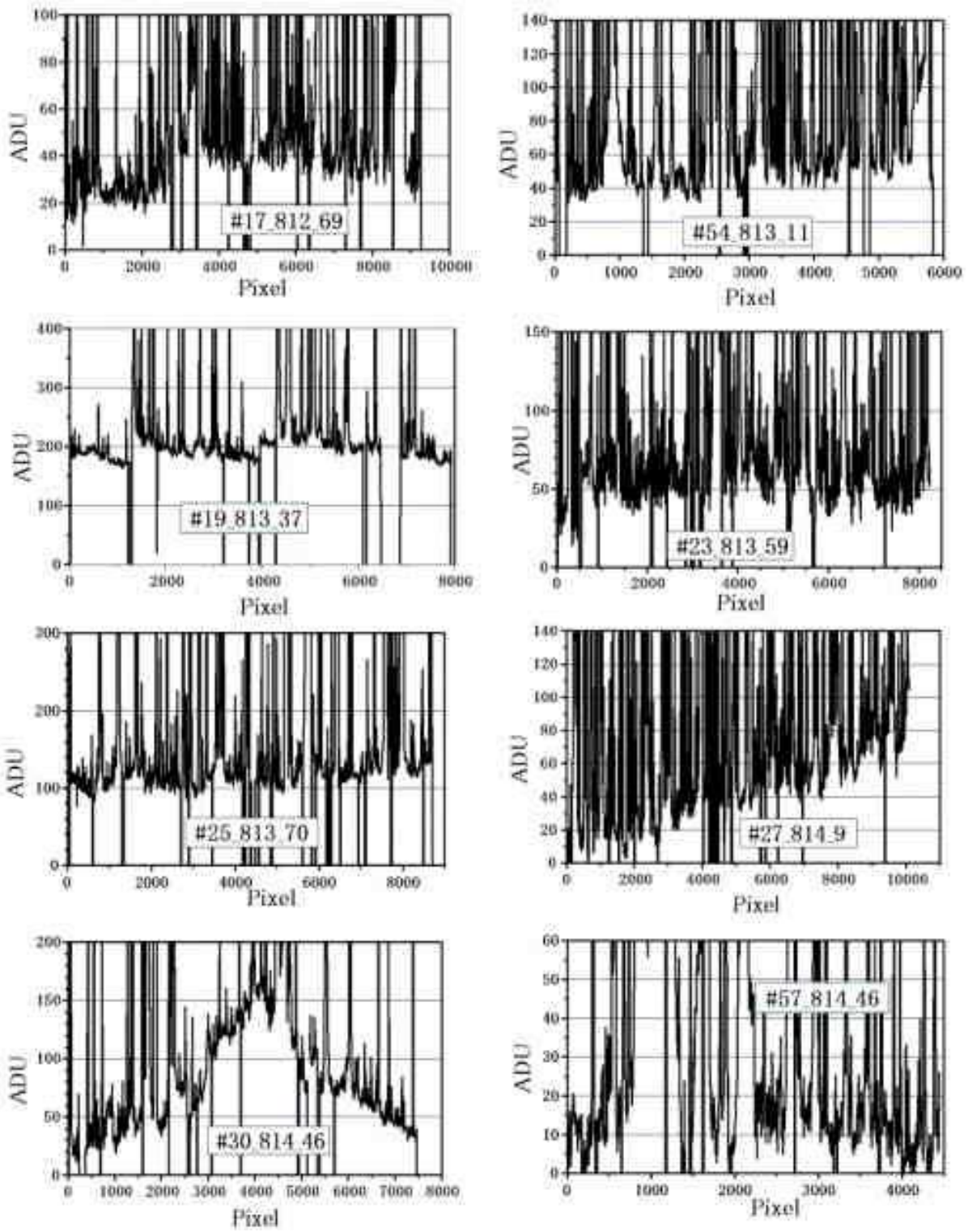


Fig. 10. Light profiles of meteors

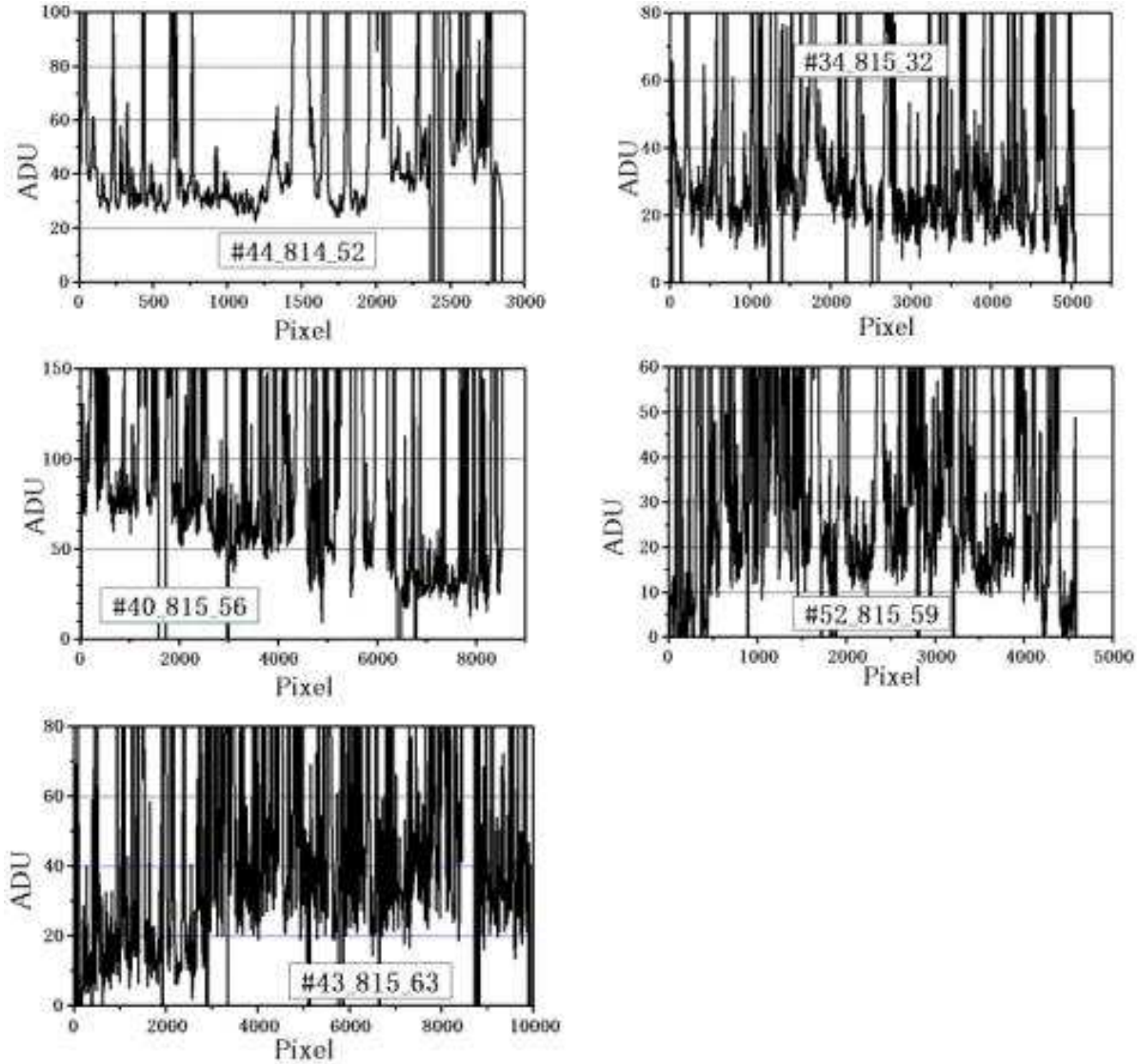


Fig. 11. Light profiles of meteors (continued)

21.6 hours, somewhat longer than the 19 hours for the current M31 observation. A total of 29 meteor events was confirmed in these SDF images. The SDF is in the constellation of Coma, where a modest meteor group was expected around 19 January. However, considering that the SDF observations were made much later than this shower period and that no other prominent meteor showers occurred during this time, we regard most of the SDF meteors as sporadic. Since we have no information that allows us to subtract possible shower events in SDF meteors, we retained all of the 29 SDF meteors as well as 13 M31 meteors in the current observation to compare their general event rates. The average event rate of SDF meteors thus obtained is 1.96 ± 0.63 times larger than, but comparable to what we obtained in the M31 field, supporting the conclusion that most of the meteors observed are also sporadic. We could not determine whether the factor of two difference in the event rate is significant.

5.2. Cross Section of the Collision Column

As shown in Figure 6, the current defocused observation cannot resolve a source size smaller than about 1m. However the following consideration gives a crude size estimate of the column cross section where the meteor collided with atmospheric atoms.

Adopting the system's photon detection efficiency of 50% by taking the optics throughput, filter transmission, and CCD quantum efficiency into account, and applying the ADC conversion factor of 2.6 e/ADC for the SuprimeCam, we can evaluate the integrated photon counts.

For example, the meteor track #19 produced a total of 5.7×10^8 photons received in the V-band by the Subaru Telescope during its 33 msec travel of $L = 2$ km length at 60km/sec and at about 100km in height, corresponding to a distance of 138km from the telescope. Assuming isotropic emission, one can derive the total number of photons emitted by this meteor during the 33msec as $N_{\text{photon}} = 2.6 \times 10^{18}$ photons. The average density of neutral oxygen atoms at a 100km height is

about $n_{OI} = 10^{18} \text{ m}^{-3}$. As a fraction η of all of the photons are emitted in [OI] 5577 by collisional excitation, this requires the effective cross section S , given by the following equation;

$$\eta N_{\text{photon}} = n_{OI} S L. \quad (10)$$

A typical meteor spectrum gives a rough estimate of the fraction of [OI] contribution in the V-band at about $\eta = 0.1$. By inserting the observed numbers for meteor #19, we obtain $S = 8.3 \times 10^{-5} \text{ m}^2$, corresponding to an effective diameter of the collision column of $D_{\text{col}} = 10.3 \text{ mm}$. The diameter of the collision column thus calculated is given for four meteors observed in the V-band in column (9) of Table 4, which is in the range of $2.4 \text{ mm} \leq D_{\text{col}} \leq 10.3 \text{ mm}$.

Note that this value represents the diameter of the column where the main body of the meteor collided with atmospheric atoms, molecules, and electrons, and where the successive cascade collisions of these particles with the neutral oxygen atoms took place. These collisions excited the neutral oxygen atoms to the energy level, which released the subsequent forbidden line [OI] 5577.

On average, the actual emission of the forbidden line occurred 0.7 sec after the collisional excitation. Therefore, the excited oxygen atoms were dispersed by thermal motions up to few hundred meters away from the original collision column before producing the forbidden-line radiation. The size of the radiating zone of the forbidden line, therefore, would be as large as few 100 m.

Note that this should be the size observed in [OI]5577 monochromatic images of meteors. The width of meteor images recorded in normal broadband frames represents the size of the hot column, which is much narrower than the [OI] wake column and would be about 1 cm – 1 m. This is consistent with the independent result of two station, short baseline observation of 34 faint meteors using intensified CCD cameras (Kaiser et al. 2004).

5.3. Radiation Efficiency and Meteor Mass

The kinetic energy E_k of a meteor particle of mass m with relative velocity to the Earth v is given by

$$E_k = mv^2/2. \quad (11)$$

Again, by assuming isotropic radiation, a photon detection efficiency of 50%, and an ADC conversion factor of 2.6 e/ADC, we can estimate the total number of photons N_{ph} emitted by the meteor during, for example, the 33msec from the video-rate ADC count F_{vr} measured by the Subaru Telescope.

$$N_{\text{ph}} = 4\pi d^2 F_{\text{vr}} / \pi R^2 \times 2.6 \times 2, \quad (12)$$

where d is the distance to the meteor and $R=4.1 \text{ m}$ is the radius of the Subaru primary mirror.

The total photon energy emitted is then

$$E_p = h\nu N_{\text{ph}}, \quad (13)$$

where $h\nu$ is the mean energy of a photon, and the conversion efficiency ϵ of thermalized energy into photons is therefore,

$$\epsilon = E_p / E_k. \quad (14)$$

Or, conversely, if we assume $\epsilon = 0.002$ Campbell-Brown and Koschny (2004), we can estimate the mass of the meteor from its magnitude as

$$m = 2E_p / v^2 \epsilon \quad (15)$$

For meteor #19, for example, $E_p = 0.94 \text{ J}$, for an average V-band photon of $3.6 \times 10^{-19} \text{ J}$. The corresponding mass would therefore be $m = 1.92 / (30,000)^2 / 0.002 = 1.1 \times 10^{-6} \text{ kg} = 1.1 \text{ mg}$

5.4. Faint meteor population and [OI] imaging

Pawlowski et al. (2001) observed very faint Leonid meteors in 1999 using an intensified CCD system mounted on a 3m liquid mirror telescope (LMT). Although their observation was sensitive down to 18 mag, the integrated magnitude along the track ranged from 5 to 10 mag, corresponding to a meteor mass of 100 to 1 μg . They estimated that the number flux of these small Leonid meteors was about 1/hour/km² perpendicular to the Leonid stream. Pawlowski's LMT observation with IICCD, covering a 0.28° field, enabled detection of 140 non-Leonid events per hour, which is astonishing. Our present observation was not as deep as their detection sensitivity due to the defocus effect of SuprimeCam. Dedicated meteor imaging with SuprimeCam focused to about 150 km distance would yield about a 3 mag gain in sensitivity and would provide important information on the faint population of meteors.

SuprimeCam Perseid radiant point imaging using an intermediate band filter IB550 to make [OI] 5577 line imaging would be useful to study the collisional excitation profile of the meteor events and their successive line emitting time profile as shown by the drifting meteor wakes. Two-dimensional images of each wake will show profiles of collisional excitation and their drifting emission. SuprimeCam should be offset by about 1.5mm to focus at 150 km distance, which is close to, but still within, the limit of the top-unit travel dynamic range. Such an observation will also give clues to the faint population of meteoroids and would be worth planning.

6. Satellites and Space Debris

Some of the tracks were promptly identified by K.Y. as artificial satellites by cross-checking with the NORAD Two-Line-Element database of registered orbit data for 8,888 satellites as of 15 August 2004, which was provided by Mike McCants via Yokohama Kagaku-kan. The possible satellites that pass the $1^\circ \times 1^\circ$ FOV centered at the telescope pointing during the 5 minute before the start of exposure and 5 minute after the end of exposure were listed up and compared to the recorded track for its position angle. Satellite tracks candidates thus identified are given their NORAD number in the fourth column of Table 5. No check was performed to determine whether the satellite was in a sunny region and thus reflected sunshine.

A separate, more extensive check was performed by C. H. at JAXA based on the Two-Line-Element data released by the NASA/GSFC Orbital Information Group. For example, Figure 12 shows the tracks of artificial objects that came close to the observed field of track#11 at the time of exposure. In this case, the artificial object, ID98077B, was confirmed to pass the SuprimeCam FOV during the 600 sec exposure time to take the image #11_812_38 along the direction of the observed track. However, the track found in Figure 13, for example, did not match to any of the 8,888 listed artificial bodies.

As shown in Table 5, seventeen tracks among the 44 non-meteor tracks coincided with recorded artificial satellites or space debris. Twenty-seven tracks, however, were not identified with an object in any available catalog. Some of these might be uncatalogued space debris objects. A possible error in orbital elements due to the secular changes of orbit, especially for low orbits objects, can also lead to cross-identification failure.

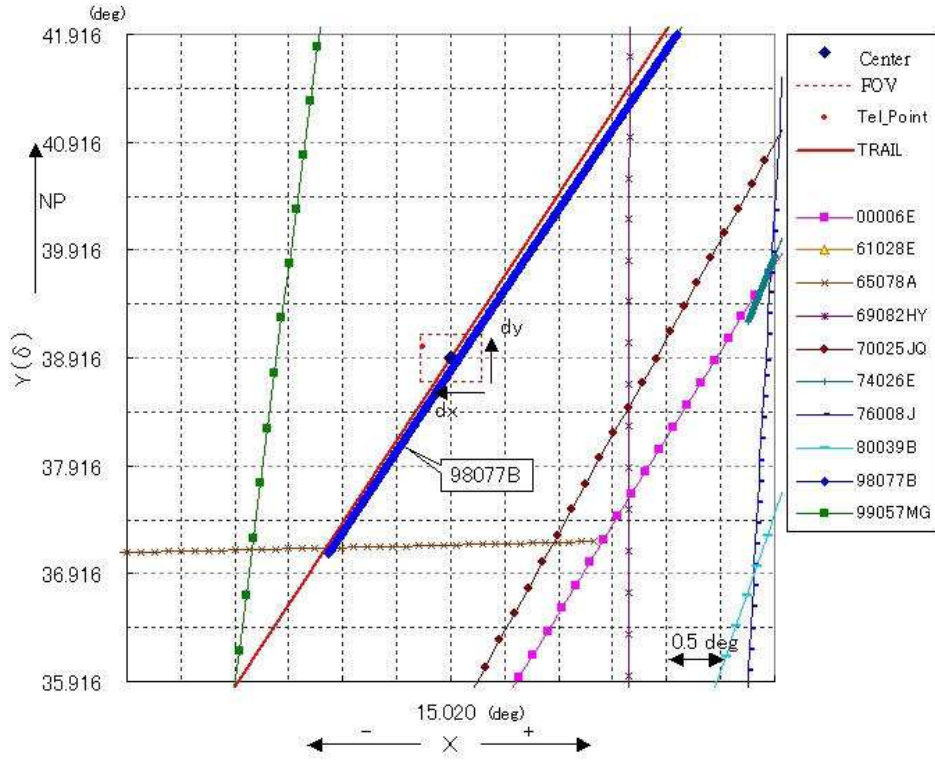


Fig. 12. Candidate orbiting satellites and debris for Track #11

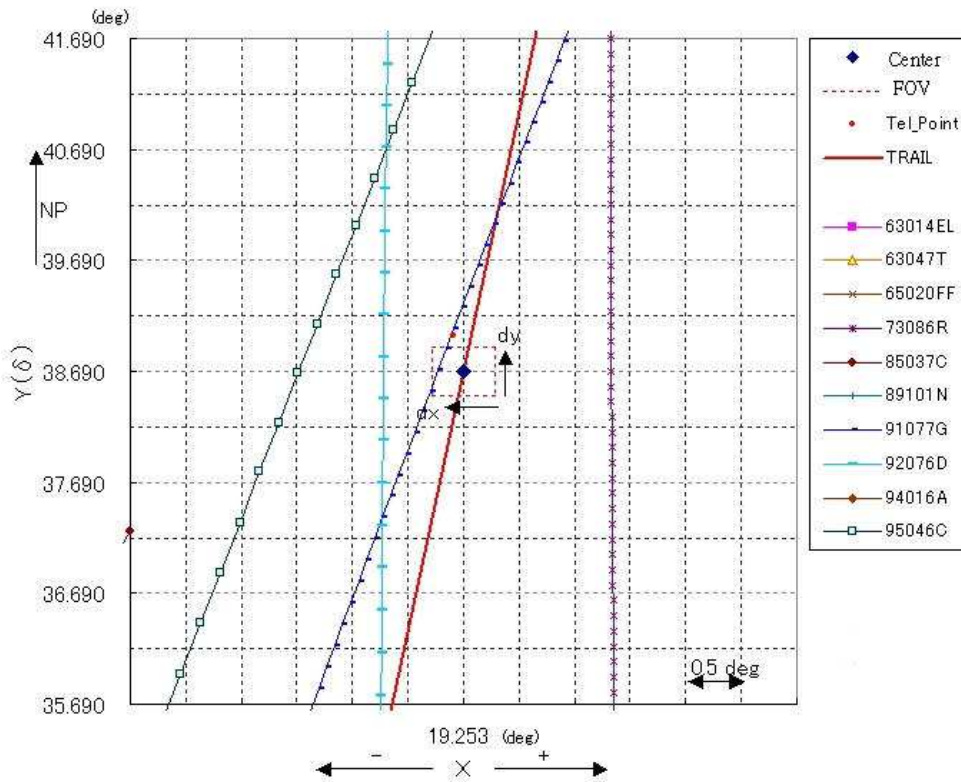


Fig. 13. Candidate orbiting satellites and debris for Track #12

(1)	(2)	(3)	(4)	(5)	(10)	(11)
#	Obs Start UTC Semi-major axis UTC (km)	ID Eccentricity	NORAD Apogee (km)	Object Name Perigee (km)	Period (min)	SlantRange (km)
1	08/11 14:03:58 7487.2	99057F 0.051	#26119 1493.6	CZ-4_DEB 724.6	107.53	1000
2	08/11 14:14:59 7315.6	75052DF 0.018	#21385 1069.7	DELTA_1_DEB 805.3	103.86	1000
3	08/12 11:53:08 9663.4	62029B 0.242	#00341 5621.7	DELTA_1_R/B 948.8	157.52	6000
4	08/12 12:04:08 23624.4	82110D 0.716	#13658 34169.0	SBS_3_R/B 323.5	602.08	25000
6	08/12 13:10:13 23080.4	83059E 0.712	#14136 33139.3	PALAPA_B1_R/B 265.3	581.41	14000
9	08/12 13:32:14 9999.5	63014M 0.019	#02362 3808.0	WESTFORD_NEEDLES 3434.8	165.92	4000
7	08/12 13:32:14 7683.2	72097B 0.027	#06306 1512.4	DELTA_1_R/B 1097.8	111.78	1200
11	08/13 10:34:14 25507.5	98077B 0.001	#25594 19160.6	COSMOS 2363 19098.1	675.73	20000
15	08/13 13:54:27 26332.4	97015D 0.630	#26764 36532.7	SL-6_R/B(2) 3375.7	708.80	13000
16	08/13 14:06:29 25997.2	93002A 0.739	#22309 38825.3	MOLNIYA_1-85 412.9	695.31	12000
46	08/13 14:06:29 72727.4	70025AM 0.003	#04653 873.1	THORAD_AGENA_D_DEB 825.4	101.93	-
22	08/14 11:37:29 25503.2	89001C 0.001	#19751 19160.4	COSMOS 1989 19089.7	675.56	20000
24	08/14 13:44:55 7502.4	63047F 0.073	#00700 1671.7	ATLAS CENTAUR 2 DEB 576.7	107.69	1500
50	08/14 14:15:07 7298.4	75010C 0.018	#07654 1049.7	DIAMANT_B-P4 790.9	103.42	-
51	08/15 11:05:00 7502.4	85118R 0.073	#23294 1671.7	SL-12_DEB 576.7	107.69	-
37	08/16 13:17:49 7780.3	94011E 0.001	#23003 1411.1	COSMOS_2272 1393.2	113.84	-
53	08/16 14:23:00 7478.1	77121X 0.007	#10580 1151.4	COSMOS_970_D 1048.5	107.27	-

Table 5. Information of identified artificial space objects based on Two Line Elements released by NASA/GSFC Orbital Information Group (Data on 08/11/2004 – 08/16/2004).

7. Conclusion

The Subaru prime focus camera, when focused to infinity, gives a conspicuously defocused image of meteors. The methods to discriminate meteors from artificial satellites/space debris were discussed. Serendipitous detection of 13 meteors during the later phase of the Perseid shower period was reported, but only 1 was securely identified as a member of the Perseids. Another meteor was ascribed to the Aquarids, but most of the remaining meteors were likely sporadic ones. Photometric magnitudes of these meteors were measured from the CCD frames by introducing a definition of video-rate magnitude to integrate flux along the tracks. Problems in linking eye-estimated magnitudes by visual observers to these photometric CCD magnitudes were discussed.

Simple calculation of the number of collisional excitations required to account for the [OI] 5577 forbidden line flux provides a new method to evaluate the diameter of the collision columns of these meteors. In this way, we derived, for the

first time, that the sizes of the collision columns of these meteors are approximately a few mm in diameter. Considering the relatively long lifetime (0.7 sec) for releasing the [OI] 5577 emission, the actual column size of the [OI] 5577 line-emitting region would be few 100m in diameter due to the thermal diffusion of excited oxygen atoms before releasing the forbidden line photons.

8. Acknowledgement

All of the meteors found were in images taken for the M31 study made by M. Chiba of Tohoku University, P. Guhathakurta of the University of California, and two of the current authors, M. I. and M. T. We are grateful to M. Chiba and P. Guhathakurta for allowing us to investigate meteor samples in the observed data. I.Iwata of NAOJ promptly provided information of tracks #1-#9 in Table 5 found during an observation preceding ours. Discussions with N.Takato of NAOJ on magnitude definition and T.Hashimoto of University

of Tokyo on line emission mechanisms were stimulating and useful. M.Horii of JAXA assisted in the orbital identification of artificial space objects.

References

- Arlt, R., 2003, WGN, Journal of International Meteor Organization, 31, 1, 19-28
- Babadzhanov, P. B. & Obrubov, I. V., 1992, Celestial Mechanics and Dynamical Astronomy, 54, 111-127
- Campbell-Brown, M. D. & Koschny, D. 2004, A& A, 418, 751-758
- Ceplecha, Z., Borovička, J., Elford, W. G., Revelle, D., Hawkes, R., Porubčan, V., & Šimek, M. 1998, Space Science Reviews, 84, 327-471.
- Cook, A., Hawkins, G. S., & Stienon, F. M. 1962, Astron. J. 67, 158-162.
- Cook, A. F., Weekes, T. C., Williams, J. T., & Omongain, E. 1980, MNRAS 193, 645-666.
- Fujiwara, Y., Ueda, M., Kawasaki, Y., & Nakamura, T. 2003, PASJ, 55, 6, 1157-1162
- Hawkins, G. S. & Whipple, F. L. 1958, Astron. J., 63, 283-291.
- Iye, M., et al. 2004, PASJ 56, 381-397
- Jenniskens, P., Jehin, E., Cabanac, R.A., Laux, C.O., & Boyd, I.D., 2004, Meteoritics & Planetary Science, 39, 609-616
- Jenniskens, P. & Stenbaek-Nielsen, H. C. 2004, Astrobiology, 4, 95-108
- Jones, J. & Sarma, T. 1979, MNRAS, 189, 225-232
- Kaiser, N., Brown, P., & Hawkes, R.L. 2004, Earth, Moon, and Planets, 95, 579-586
- Kondrat'eva, E. D., & Ishmukhametova, M. G., 2004, WGN, Journal of International Meteor Organization, 32, 54-56
- Landolt, A. U. 1992, AJ, 104, 340-371, 436-491,
- Lindblad, B.A., & Porubcan, V. 1995, Earthe, Moon, and Planets, 68, 409-418
- Lyytinen, E. & Van Flandern, T. 2004, <http://www.metaresearch.org/solar%20system/perseid/perseids.asp>
- Lyytinen, E. & van Flandern, T. 2004, WGN, Journal of the International Meteor Organization, 32, 2, 51-53
- Miyazaki, S., et al. 2002, PASJ, 54, 833-853
- Molau, S & Arlt, R. 1997, Planetary and Space Organization, 45, 857-864.
- Nakamura, R., Fujii, Y., Ishiguro, M., Morishige, K., Yokogawa, S., Jenniskens, P., & Mukai, T. 2000, ApJ, 540, 1172-1176
- Ouchi, M., et al. 2004, ApJ, 611, 660-684
- Pawlowski, J. F., .Hebert, T. J., Hawkes, R., L., .Matney, M. J., & Stansbery, E. G., 2001, Meteor & Planetary Science, 36, 1467-1477
- Sato, M. 2004, <http://kaicho.pobox.ne.jp/tenshow/meteor/109p/2004.htm>
- Shiba, Y., Ohtsuka, K., & Watanabe, J. 1993, Proc. International Astronomical Symposium held at Smolenice, eds. J.Stohl and I.P.Williams, p189.
- Yagi, M., Kashikawa, N., Sekiguchi, M., Doi, M., Yasuda, N., Shimasaku, K., & Okamura, S. 2002, AJ, 123, 66-86.
- Yanagisawa, T., Ohnishi, K., Torii, K., Kohama, M., Nakajima, A., & Asher, D., 2003, PASJ, 55, 553-557